

Translated from: ZHANG Y H, CHEN C H, ZHU X. GFRP and steel compounded structure subjected to impact by high velocity projectiles[J]. Chinese Journal of Ship Research, 2017, 12(1): 93-100.

GFRP and steel compounded structure subjected to impact by high velocity projectiles

ZHANG Yuanhao, CHEN Changhai, ZHU Xi

Department of Naval Architecture Engineering, Naval University of Engineering, Wuhan 430033, China

Abstract: To explore the influence of steel and GFRP structural configuration on the perforation-resistance of a composite armor system of warship bulkhead, a series of high velocity ballistic impact experiments are performed. The outer and inner composite armor systems of warship bulkhead are simulated using homogeneous steel plates prefaced and backed with composite laminates, respectively. Failure modes and energy absorption for the two types of combined targets are analyzed and compared with each other. Based on the experimental results, the compounded structure subjected to the impact caused by cube projectiles is simulated using finite element program ANSYS/LS-DYNA, where the process of penetration is investigated and compared with experiment results. It is observed that the numerical results are in good agreement with the experimental results; the failure modes for the composite armors in the two types of combined targets are mainly the shear punch failure of steel plates and the fiber shear fracture of GFRP, while the GFRP in the combined target consisting of front steel plates and composite backed armors also has tensile failure of fibers; the combined target consisting of front steel plates and composite backed armors absorbs much more energy than that consisting of front composite armors and steel backed plates.

Key words: warship bulkhead; composite armor; ballistic performance; GFRP and steel compounded structure

CLC number: U661.43; O344.7

0 Introduction

With the continuous development of anti-ship missile, sea-skimming semi-armor-piercing anti-ship missile due to its characteristics of outstanding penetration ability, topside implosion and so on, has become the main threat to modern ships. The high velocity fragments from the implosion of warhead would cause the secondary damage to the important cabins of ship, so the protection issue of kinetic-energy perforation resistibility of warship bulkhead is particularly prominent. At present, for the kinetic-energy perforation effect of high velocity fragments, to increase the bulkhead thickness and to employ the composite armor are the main engineering solutions to reduce the damage to cabins.

For the kinetic-energy perforation effect of high

velocity fragments produced by the implosion of semi-armor-piercing warhead, the modern warship cabin usually adopts the setup of composite armor structure. Fiber reinforced plastics (FRP) due to its advantages of high specific strength and specific stiffness has been widely used in the warship composite armor protection structure^[1-2]. But the laminated structure and the complexity of the material properties cause the ballistic impact process very complex, with a lot of influencing factors. Scholars are committed to thoroughly investigate the dynamic mechanical deformation mechanism of the composite target material during the penetration and perforation process. For the perforation resistance issue of a single composite material plate or a homogeneous steel plate, there have been a lot of research accomplished at home and abroad^[3-5]. The investigation of the an-

Received: 2016 - 03 - 16

Supported by: National Natural Science Foundation of China (51409253)

Author(s): ZHANG Yuanhao, male, born in 1992, master candidate. Research interest: protection of warships.

E-mail: 158241904@qq.com

CHEN Changhai (Corresponding author), male, born in 1985, Ph. D., lecturer. Research interests: explosion and penetration resistance of warship structure. E-mail: chenchanghai@126.com

ZHU Xi, male, born in 1961, Ph. D., professor. Research interests: material structural mechanics, composite, and explosion and shock resistance of warship structure. E-mail: zhuxi816@163.com

ti-penetration property of FRP, Greaves^[6-7] used the flat-nosed projectile to hit S2 Glass/Phenolic laminated thick target and studied the failure mechanism in the process of ballistic perforation; Zhu et al.^[8-9] studied the energy adsorption mechanism when the cylindro-conical projectile hit the Kevlar-29/Polyester laminated plate; Wen et al.^[10-12] put forward the penetration depth and ballistic limit formulas when different shapes of projectiles penetrated FRP laminated plates. Qin et al.^[13] evaluated the perforation performance when ogival-nosed projectile impacted the FRP laminated plates; Zhang et al.^[14] introduced the damage performance characterization method for FRP laminated plates; Xie et al.^[15] employed the finite element method to simulate the dynamic response when different fragments penetrated Glass Fiber Reinforced Plastics (GFRP) laminated plates. For the combination target of the fiber reinforced composite plates and the homogeneous steel plates, there is barely ongoing research.

The warship bulkhead structure belongs to the medium plate relative to the high velocity fragments, so the high velocity fragment penetration to the warship bulkhead structure can be considered as the high velocity perforation resistance issue of medium plate. In order to study the failure mechanism difference of kinetic-energy perforation resistibility between the inner and outer composite armor structures of the warship bulkhead and compare the perforation-resistance of the inner and outer composite armor structures, this article used the homogeneous steel plate prefaced and backed with GFRP to simulate the outer and inner composite armor structures, combined with high velocity ballistic impact experiment, to analyze and compare the failure modes and the ballistic performance of the front and composite backed armors. Based on this, the finite element analysis software ANSYS/LS-DYNA was used to carry out the numerical simulation of the high velocity cube projectile penetrating the combined target. The penetration process and failure mode of the combined target were analyzed, which were compared with the corresponding experimental results.

1 Experiment and Results

During the experiment, we used 14.5 mm caliber of smoothbore ballistic rifle system to launch projectile bodies, which was pushed by the gunpowder. In order to ensure the required sealing and the necessary launching velocity, fragments were clad with the special three-lobe aluminum alloy sabot. The

sabots were separated by the sabot recoverer when the fragments were out of the chamber, and the fragment motion trajectory was kept at the same time. The system includes a laser velocity measuring device.

The cube projectile had the side length of 7.5 mm and the design mass of 3.30 g, and the projectile body was obtained after quenching treatment of 45[#] steel.

Q235 steel was used as the steel target, and the square target had the size of 400 mm × 400 mm × 5 mm, exposure area of 300 mm × 300 mm and surface density of 39 kg/m²; the GFRP target is made of SW220 glass fiber cloth with the dimension of 200 mm × 200 mm × 5 mm and the surface density of 12 kg/m². The epoxy resin was used to adhere the above two targets. The fixed target frame was used in the experiment. The target frame was fixed on the slide. In the process of experiment, the target was fixed to the target frame.

The material parameters of 45[#] steel, Q235 steel and SW220 GFRP were summarized in Table 1 and Table 2.

Table 1 Material properties of steel

Parameter	Value	
	45 [#] steel	Q235 steel
Elastic modulus E /GPa	205	210
Density ρ /(kg·m ⁻³)	7 800	7 850
Poisson's ratio ν	0.3	0.3
Stress σ_y /MPa	335	235
Tensile strength σ_b /MPa	450	400-490
Elongation δ_s /%	16	22

Table 2 Material properties of SW220 GFRP

Parameter	Value
Density ρ /(kg·m ⁻³)	2 100
In-plane tensile modulus/GPa	30.5
In-plane tensile strength/MPa	450
Compression modulus in thickness direction/GPa	3.85
Compression strength in thickness direction/MPa	488.3
Shear modulus/GPa	1.11
Shear strength/MPa	156
Fracture toughness value/(J·cm ⁻²)	1.59
Elongation δ_s /%	1.5
Unit fracture strain energy/(MJ·m ⁻³)	3.38

2 Finite Element Simulation Results

By using finite element software LS-DYNA, the numerical simulation model of the high velocity projectile penetrating the combined target was established. The projectile and the target adopted

eight-node Lagrange entity unit for simulation. The Lagrange grid modeling was used, and the projectile was equally divided into 8 segments on each side; we selected a square area with the size of 50 mm × 50 mm in the center of the target. The grid refinement processing was carried out in the impact area, which was further equally divided into 50 parts on each side. Away from the region, the grids made the sparse transition to target corners and the target thickness direction was equally divided into 10 parts. The grid model is shown in Fig. 1.

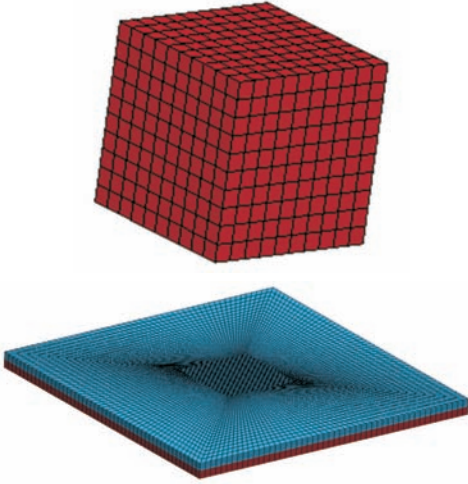


Fig.1 Sketch of finite element model for cube projectile and steel /GFRP compounded structure

The projectile uses the bilinear elastoplastic constitutive model (Plastic_Kinematic) and its strain rate effect should be described by Cowper–Symonds model:

$$\sigma_d = \left(\sigma_0 + \frac{EE_h}{E - E_h} \varepsilon_p \right) \left[1 + \left(\frac{\dot{\varepsilon}}{D} \right)^{1/N} \right]$$

where σ_d is the dynamic yield strength; σ_0 is the static yield strength; E is the elastic modulus; E_h is the hardening modulus; ε_p is the effective plastic strain; $\dot{\varepsilon}$ is the equivalent plastic strain rate; D and N are constant; for low carbon steel, D usually takes 40.4 s⁻¹, and N takes 5. Material failure model uses the criterion of maximum equivalent plastic strain failure.

Material parameters^[16] of projectile are summarized in Table 3.

Table 3 Material parameters of projectile

σ_0 /MPa	E_h /MPa	N	D /s ⁻¹	Failure strain ε_f
335	350	5	40.4	0.7

Steel plate uses Johnson–Cook constitutive model and the model considers the strain rate strengthening and the softening effect caused by the adiabatic heat-

ing, which can reflect the material properties change under the condition of high strain rate and high temperature. The state equation is shown as below:

$$\sigma_y = (A + B\varepsilon^{pn}) \left[1 + c \ln \frac{\dot{\varepsilon}^p}{\varepsilon_0} \right] \left[1 - \left(\frac{T - T_0}{T_m - T_0} \right)^m \right]$$

where σ_y is the dynamic yield strength of the steel plate; A is the static yield strength which is 235 MPa; B is the strain hardening modulus which is 300 MPa; n is the strain hardening index which is 0.26; c is the strain rate coefficient which is 0.014; m is the thermal softening index which is 1.03; ε^p is the equivalent plastic strain; ε_0 is the reference plastic strain rate which is usually 1 s⁻¹; T_m is the melting point of material which is 1 793 K; and T_0 is the reference temperature (ambient temperature) which is 300 K.

The material failure of the impact area can be described by the following equation:

$$\varepsilon_f = \left[D_1 + D_2 \exp \left(D_3 \frac{\sigma_h}{\sigma_{\text{eff}}} \right) \right] \left(1 + D_4 \frac{\dot{\varepsilon}^p}{\dot{\varepsilon}_0} \right) \left[1 + D_5 \left(\frac{T - T_0}{T_m - T_0} \right) \right]$$

where $D_1 - D_5$ are material constant; σ_{eff} is the equivalent Mises stress; σ_h is the hydrostatic pressure of material under three-dimensional stress state; when the damage parameter $D = \sum \frac{\Delta \varepsilon^p}{\varepsilon_f} = 1$, the material failure occurs. Material parameters^[16] of steel plate are shown in Table 4, where G is the shear modulus.

Table 4 Material parameters of steel plate

G /GPa	A /MPa	B /MPa	n	c	m	T_m /K	T_0 /K	D_1	D_2	D_3	D_4	D_5
80.8	235	300	0.26	0.014	1.03	1 793	300	0.4	0	0	0	0

GFRP uses Johnson–Cook Composite–Damage constitutive model and the stress–strain relationship for the model material is described below:

$$\begin{cases} \varepsilon_1 = \frac{1}{E_1} (\sigma_1 - \nu_1 \sigma_2) \\ \varepsilon_2 = \frac{1}{E_2} (\sigma_2 - \nu_2 \sigma_1) \\ 2\varepsilon_{12} = \frac{1}{G_{12}} \tau_{12} + \alpha \tau_{12} \end{cases}$$

where ε_1 , ε_2 , and ε_{12} are longitudinal tensile strain, transverse tensile strain and in-plane shear strain, respectively; σ_1 , σ_2 , and τ_{12} are the longitudinal tensile stress, transverse tensile stress and in-plane shear stress, respectively; ν_1 and ν_2 are the longitudinal and transverse Poisson's ratios, respectively; E_1 , E_2 and G_{12} are the longitudinal tensile modulus, transverse tensile modulus and in-plane shear

modulus, respectively; and α is the nonlinear shear stress parameter.

The model adopts 3 failure criteria of Chang–Chang failure criterion as follows:

1) Matrix cracking failure criterion:

$$F_{\text{matrix}} = \left(\frac{\sigma_2}{S_2}\right)^2 + \bar{\tau}$$

When $F_{\text{matrix}} > 1$, the matrix cracking failure occurs, and the material constants E_1 , E_2 , v_1 and v_2 are all zero.

2) Compression failure criterion:

$$F_{\text{comp}} = \left(\frac{\sigma_2}{S_{12}}\right)^2 + \left[\left(\frac{C_2}{2S_{12}}\right)^2 - 1\right] \frac{\sigma_2}{C_2} + \bar{\tau}$$

When $F_{\text{comp}} > 1$, the material compression failure occurs, and the material constants E_2 , v_1 and v_2 are all zero.

3) The ultimate failure mode is fiber fracture.

$$F_{\text{fiber}} = \left(\frac{\sigma_1}{S_1}\right)^2 + \bar{\tau}$$

When $F_{\text{fiber}} > 1$, the fiber fracture failure occurs, and the material constants E_1 , E_2 , G_{12} , v_1 and v_2 are all zero. Material parameters of GFRP are shown in Table 5.

Table 5 Material parameters of GFRP

E_{11}/GPa	E_{22}/GPa	E_{33}/GPa	v_{12}	v_{13}	v_{23}	G_{12}/GPa	G_{13}/GPa	G_{23}/GPa
18.22	18.22	6	0.12	0.3	0.3	6.75	6.75	3

Based on the observation of the experimental results, we find that the projectile penetration is perpendicular to the target. The ballistic experiment and numerical simulation results as well as the related parameters are shown in Table 6. The target type I is combined target of 5 mm GFRP + 5 mm steel plate, and the target type II is combined target of 5 mm steel plate + 5 mm GFRP.

Table 6 Results of finite element and experiment

Experiment condition	Target type	Projectile velocity v_0 /($\text{m}\cdot\text{s}^{-1}$)	Residual velocity /($\text{m}\cdot\text{s}^{-1}$)	Energy absorption in unit surface density $E_A/(\text{J}\cdot\text{m}^2\cdot\text{kg}^{-1})$	Residual velocity by numerical simulation/($\text{m}\cdot\text{s}^{-1}$)	Relative error/%	Damage situation
1	I	1 057.2	0	≥ 36.16	0	—	GFRP was perforated and steel plate was critically perforate
2	II	1 001.2	0	≥ 32.43	0	—	Steel plate was perforated and GFRP was critically perforate
3	I	1 194.4	327.8	42.68	343	4.6	Overall perforated; both the steel plate and GFRP were perforated
4	II	1 291.7	617.7	41.64	628	1.7	Overall perforated; both the steel plate and GFRP were perforated

3 Experiment and Calculation Results Analysis

3.1 The target penetration process and failure mode analysis

3.1.1 The experimental result of target type I

In failure mode 1, the damage morphologies of the front GFRP and the steel backed plate are shown in Fig. 2. As shown in the picture, the front FRP under the projectile penetration shows the fiber degumming phenomenon. The dominant perforation failure mode of projectile is the shear fracture failure of the fiber, and the fiber fracture shows a neat surface. While, the perforation failure mode of the steel backed plate is mainly shear punch failure. Because of the low velocity of projectile after perforating the front GFRP, the fragments do not entirely perforate through the steel backed plate. The shear block has not separated from the steel plate, inducing a local uplift at the fragment perforation part of steel plate.



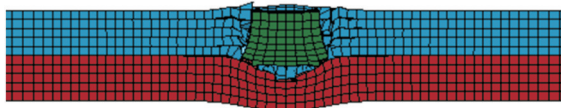
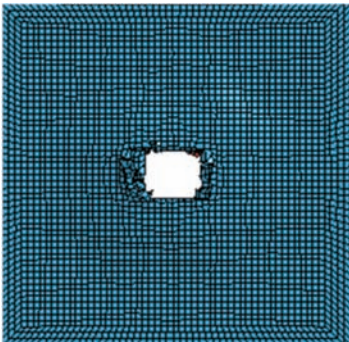
(a) Front surface of GFRP



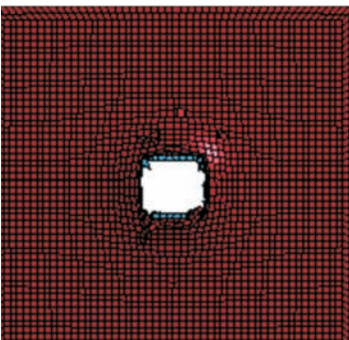
(b) Back surface of steel plate

Fig.2 Failure mode 1

Fig. 3 shows the finite element simulation of failure mode 3. As shown in the figure, the projectile has made the GFRP fractured in the fiber layer in the process of penetration, causing the shear failure (Fig. 3 (a)). Projectile continued to penetrate to the steel plate and the high velocity penetration produced shock wave. The shock wave reflection caused the projectile erosion. Thus, the projectile further upset and the penetration velocity declined obviously. The local fiber degumming phenomenon of GFRP occurred in the penetration area (Fig. 3 (b)). Failure

(a) $t = 12 \mu\text{s}$ (b) $t = 21 \mu\text{s}$ (c) $t = 33 \mu\text{s}$ (d) $t = 40 \mu\text{s}$ 

(e) Front surface of GFRP



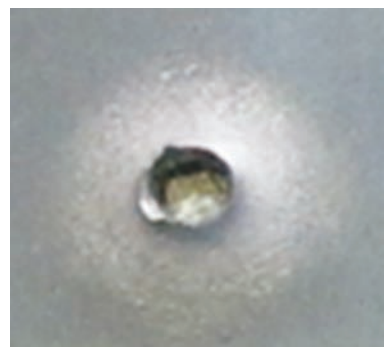
(f) Back surface of steel plate

mode of steel plate is shear failure. In the whole course of projectile penetration, the steel plate unceasingly absorbed the projectile penetration energy, and the projectile velocity continued to decline. In the later stage of penetration, the steel plate has failed, and the projectile also appeared continuous upsetting until it perforated the whole steel backed plate (Fig. 3 (d)).

In failure mode 3, the projectile completely perforated through the target, and the damage morphologies of target is shown in Figure 4. As seen from Fig. 3(e) and Fig. 4, compared with failure mode 1, the perforation part of front GFRP not only had fiber shear fracture, but also appeared a lot of fiber degumming around the perforation as well as fibrillation after the fiber fracture. It is mainly because under the high velocity, the projectile would have significant friction with the fiber in the process of shear perforation, and the heat generated by friction is not easy to be transferred, causing the fiber massively fused. By observing the damage morphology of the steel backed plate and the color of the target around the perforation area, and combined with Fig. 3 (f), it was found out that the failure mode is shear punch failure and the shear punch perforation area has a certain degree of plastic deformation. It is mainly because that the front GFRP reduced the velocity of the projectile when impacting the steel backed plate, and the fractured fiber adhered to the warhead sur-



(a) Front surface of GFRP



(b) Back surface of steel plate

Fig.3 Penetration process simulation of failure mode 3

Fig.4 Failure mode 3

face to increase the impact area of the projectile on the steel backed plate.

3.1.2 The experimental result of target type II

The damage morphology of the target in failure mode 2 is shown in Fig. 5. As shown in the figure, the front steel plate has obvious shear punch phenomenon on the edge of the impact zone and the impact zone periphery has a large amount of deformation. Thus, the main failure mode is shear plugging. The perforation shape of the steel plate is approximately circular, and the material around the perforation shows "reverse overflowing" phenomenon, which is due to the extrusion of the approximately fluid-like target material when the projectile perforated the armor. But the backed GFRP was not totally perforated, and the failure mode is fiber shear fracture on the front surface and delamination fracture on the back surface. As seen from the damage morphology of backed GFRP, the back layer exhibited the fiber degumming phenomenon around the penetrated hole, and the back unperforated fiber layer showed the delamination and local deformation.



(a) Front surface of steel plate



(b) Back surface of GFRP

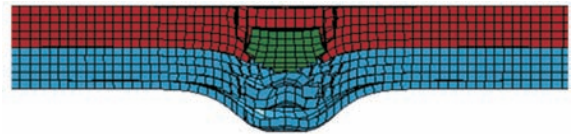
Fig.5 Failure mode 2

Penetration process simulation of failure mode 4 is shown in Fig. 6. As seen from the figure, the projectile contacted with the steel plate to have the shear failure. At the same time, the projectile showed upsetting (Fig. 6(a)). After the steel plate failed, the projectile penetration load was transferred

to the GFRP. Under the penetration loading, the back fiber of GFRP exhibited spallation, accompanied by shear and tensile damage of fiber. In the process of penetration, the penetration energy of the projectile was absorbed continuously, causing the continuous decline of velocity (Fig. 6(b)). The steel plate plug block continued to erode the projectile between the projectile and the GFRP, and the back fiber layer was completely destroyed and lost protection capability. The projectile accompanied with the steel plate and the fiber impact block perforated the



(a) $t = 9 \mu\text{s}$



(b) $t = 15 \mu\text{s}$



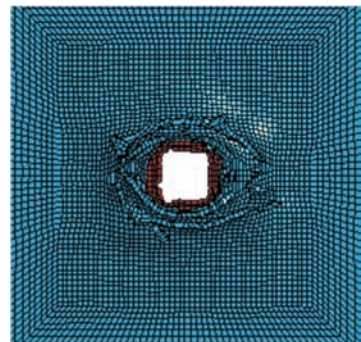
(c) $t = 18 \mu\text{s}$



(d) $t = 23 \mu\text{s}$



(e) Front surface of steel plate



(f) Back surface of GFRP

Fig.6 Penetration process simulation of failure mode 4

target (Fig. 6(d)).

The damage morphology of target in failure mode 4 is shown in Fig. 7. As seen from the figure, the damage of the backed GFRP is more severe than that in the failure mode 2. Combined with Fig. 6(f), it mainly shows that the unperforated fiber layer on the back layer has fiber layer degumming and fibrillation phenomenon, accompanied by obvious fiber tensile failure. From Fig. 7(a) and Fig. 6(e), the failure mode for the front steel plate is the shear punch failure.



(a) Front surface of steel plate



(b) Back surface of GFRP

Fig.7 Failure mode 4

3.2 The residual velocity results comparison

Table 6 shows the residual velocity results from experiment and finite element simulation, and in the finite element simulation, the initial velocity of projectile is consistent with the experimental condition. As seen from the table, when the initial velocity is high (failure modes 3 and 4), the relative error of residual velocity from the experiment and finite element simulation is small, demonstrating that the results of numerical simulation are reliable. The initial velocities of projectile in failure mode 3 and failure mode 4 have little difference, but the residual velocity of failure mode 4 is nearly twice that of failure mode 3. When the initial velocity of projectile is about 1 000 m/s, as shown in Fig. 2(b), the convex closure of the steel backed plate has cracks and only a small part was not separated from the steel plate,

which is in the critical penetrated state. As observed in Fig. 5(b), the projectile has perforated to the last fiber layer of the GFRP. So, by analyzing the deformation failure of the steel backed plate after experiment and the finite element simulation, it is approximately considered that the target type I when $v_0 = 1\ 050$ m/s and the target type II when $v_0 = 1\ 000$ m/s have reached the ballistic limit state.

3.3 Comparative analysis of penetration resistance of the target

It has been mentioned in the above section that the ballistic limits of target type I and target type II are about 1 050 and 1 000 m/s. Therefore, from the ballistic limit perspective, target type I is slightly better than type II. Further comparison of failure mode 3 and failure mode 4 shows that, for two types of combined targets under the similar initial velocity of projectile, the former has an energy absorption value in unit surface density of 42.68 ($\text{J} \cdot \text{m}^2$)/kg, and the latter has a value of 41.64 ($\text{J} \cdot \text{m}^2$)/kg. Thus, it can be seen that the energy absorption of target type I is higher than that of target type II. This is mainly because that when the projectile penetrated into the combined target of GFRP + steel plate, on one hand, the dynamic support of steel backed plate on the GFRP increased the local inertial mass of the projectile during the penetration process; on the other hand when the projectile penetrated into the front GFRP, the compressive stress wave produced by the projectile penetration was transmitted to the steel backed plate, which makes the steel backed plate participate in energy absorption and generate compression work. But when the projectile penetrated the combined target of steel plate + GFRP, the compressive stress wave made the back layer of GFRP have slight inter-layer degumming phenomenon during the penetration process (Fig. 5(b)). This would reduce the penetration resistance performance of the backed GFRP, and reduce the overall penetration resistance performance of the combined target of steel plate + GFRP to some extent.

4 Conclusions

In this article, the high velocity ballistic impact experiment and the numerical simulation with finite element analysis software ANSYS/LS-DYNA was used to analyze and compare the failure mode and energy absorption ability of two kinds of combined targets, the following conclusions have been drawn:

1) Under the penetration of the high velocity cube

projectile, the failure mode of the combined target of steel plate + GFRP is shear punch failure. The GFRP failure mode is mainly shear fracture of the fiber, and the back layer of GFRP shows the fiber interlayer degumming and tensile failure.

2) Under the penetration of the high velocity cube projectile, in the combined target of GFRP + steel plate, the failure mode of steel plate is the shear punch failure, and the GFRP failure mode is shear fracture of the fiber.

3) Under the penetration of the high velocity cube projectile, due to the support of the steel backed plate and the influence of the compressive stress work, the penetration resistance of the combined target of GFRP + steel plate is slightly better than that of the combined target of steel plate + GFRP.

References

- [1] ZHU X, MEI Z Y, LIU R Q, et al. Warship's light composite armor structure resistibility for ballistic impact [J]. *Explosion and Shock Waves*, 2003, 23 (1) : 61-66 (in Chinese).
- [2] ZHU X, HOU H L, GU M B, et al. Experimental study on armor protection against ballistic impact of small caliber artillery [J]. *Explosion and Shock Waves*, 2006, 26(3) : 262-268 (in Chinese).
- [3] MEI Z Y, ZHU X, LIU Y H, et al. The developments of fibre-reinforced composite laminates under ballistic impact [J]. *Advances in Mechanics*, 2003, 33 (3) : 375-388 (in Chinese).
- [4] WANG X Q, ZHU X, MEI Z Y. The development of fiber-reinforced composites under ballistic impact [J]. *Fiber Reinforced Plastics/Composites*, 2008 (5) : 47-56 (in Chinese).
- [5] WANG X Q, ZHU X. Review on ballistic impact resistance of ship building steel [J]. *Shipbuilding of China*, 2010, 51(1) : 227-236 (in Chinese).
- [6] GREAVES L J. Failure mechanisms in GFRP armour [R]. UK: Unpublished UK DRA Report, 1992.
- [7] GREAVES L J. Progress in modeling the perforation of GFRP by ballistic projectiles [R]. UK: Unpublished UK DRA Report, 1994.
- [8] ZHU G Q, GOLDSMITH W, DHARAN C K H. Penetration of laminated Kevlar by projectiles-I. experimental investigation [J]. *International Journal of Solids and Structures*, 1992, 29(4) : 399-420.
- [9] ZHU G Q, GOLDSMITH W, DHARAN C K H. Penetration of laminated Kevlar by projectiles-II. analytical model [J]. *International Journal of Solids and Structures*, 1992, 29(4) : 421-436.
- [10] WEN H M, REDDY T Y, REID S R, et al. Indentation, penetration and perforation of composite laminate and sandwich panels under quasi-static and projectile loading [J]. *Key Engineering Materials*, 1998, 141/142/143 : 501-552.
- [11] REDDY T Y, WEN H M, REID S R, et al. Penetration and perforation of composite sandwich panels by hemispherical and conical projectiles [J]. *Journal of Pressure Vessel Technology*, 1998, 120(2) : 186-194.
- [12] REID S R, WEN H M, SODEN P D, et al. Response of single skin laminates and sandwich panels to projectile impact [C]//WANG S S, WILLIAMS J J, LO K H. *Composite materials for offshore operation-2*. [S. l.]: American Bureau of Shipping, 1999: 593-617.
- [13] QIN Y, WEN H M, HE T. Penetration and perforation of FRP laminates under normal impact by ogival-nosed projectiles [J]. *Acta Materiae Compositae Sinica*, 2007, 24(2) : 131-136 (in Chinese).
- [14] ZHANG Y J, MEI Z Y, ZHU X. Current status and prospects of study on low velocity impact damaged characterization of fiber-reinforced composite laminates [J]. *Fiber Reinforced Plastics/Composites*, 2011 (1) : 52-58 (in Chinese).
- [15] XIE H, LV Z H. Finite element simulation of FRP plates impacted by fragments [J]. *Journal of Tsinghua University (Science & Technology)*, 2012, 52(1) : 96-101 (in Chinese).
- [16] LI M, ZHU X, HOU H L, et al. Numerical simulation of steel plates subjected to the impact of both impact waves and fragments [J]. *Chinese Journal of Ship Research*, 2015, 10(6) : 60-67 (in Chinese).

钢/玻璃钢组合结构对高速弹丸的抗侵彻特性

张元豪, 陈长海, 朱锡

海军工程大学 舰船工程系, 湖北 武汉 430033

摘要: 为探究钢与玻璃钢的组合结构形式对舰船舱壁复合装甲结构抗穿甲性能的影响, 采用均质钢板前置和后置玻璃钢来分别模拟舰船舱壁外设及内设复合装甲结构, 结合高速弹道冲击实验, 分析、比较2种结构形式组合靶板的穿甲破坏模式和抗弹吸能能力。在此基础上, 利用有限元分析软件 ANSYS/LS-DYNA 开展高速立方体弹丸侵彻组合靶板的数值模拟计算, 分析组合靶板的侵彻过程, 并与实验结果进行比较。结果表明, 数值计算结果与实验结果较为吻合; 2种组合靶板中复合装甲板的破坏模式均主要为钢板的剪切冲塞破坏和玻璃钢的纤维剪切断裂, 后置组合靶板中玻璃钢背层伴随有纤维的拉伸破坏; 前置组合靶板的抗弹吸能能力要稍大于后置组合靶板。

关键词: 舰船舱壁; 复合装甲; 抗弹性能; 钢/玻璃钢组合结构